Shihora, L., Balidakis, K., Dill, R., Dobslaw, H. (2023): Assessing the stability of AOD1B atmosphere-ocean non-tidal background modelling for climate applications of satellite gravity data: long-term trends and 3-hourly tendencies. - Geophysical Journal International, 243, 2, 1063-1072.

https://doi.org/10.1093/gji/ggad119

Geophysical Journal International

Geophys. J. Int. (2023) **234,** 1063–1072
Advance Access publication 2023 March 21
GJI Gravity, Geodesy and Tides

https://doi.org/10.1093/gji/ggad119

Assessing the stability of AOD1B atmosphere–ocean non-tidal background modelling for climate applications of satellite gravity data: long-term trends and 3-hourly tendencies

Linus Shihora, Kyriakos Balidakis, Robert Dill and Henryk Dobslaw

GFZ German Research Centre for Geosciences, 1.3 *Earth System Modelling,* 14473 *Potsdam, Germany. E-mail: linus.shihora@gfz-potsdam.de*

Accepted 2023 March 14. Received 2023 March 3; in original form 2023 January 6

SUMMARY

The GRACE Atmosphere and Ocean Level-1B (AOD1B) product is routinely applied in the processing of satellite gravimetry data to mitigate the impact of temporal aliasing. Spurious trends, low-frequency signals or bias jumps in the background model data can, if unaccounted for, introduce biases into the global gravity solutions which might be interpreted erroneously in subsequent geophysical analyses. Here, we examine the most recent release, RL07, of AOD1B for such artefacts. A focus is placed on the transition from the atmospheric re-analysis ERA5 to operational weather model data, in January 2018, which coincides with the gap between the missions GRACE and GRACE-FO. We find that linear trends computed from 1975 to 2020 are well below 30 Pa a^{-1} for all components of RL07. The assessment of 3-hourly tendencies gives no indication of bias jumps and shows that the transition in atmospheric data does not have an adverse effect on the consistency of RL07. We conclude with a comparison of the variability of both AOD1B RL06 and RL07 in the context of their application in satellite gravimetry.

Key words: Global change from geodesy; Satellite geodesy; Satellite gravity; Time variable gravity; Time-series analysis.

1 INTRODUCTION

Satellite gravimetry missions such as GRACE (Tapley *et al.* 2004) and its successor GRACE-FO (Landerer *et al.* 2020) have provided invaluable insight into Earth's large-scale mass variations. Monthly gravity solutions covering more than 20 yr have been extensively used to monitor changes in terrestrial water storage (TWS; Rodell *et al.* 2018), ice-mass loss in Greenland (Sasgen *et al.* 2020) and Antarctica (Velicogna & Wahr 2006) as well as ocean mass variability (Chen *et al.* 2018) associated with the inflow of water from the continents. A thorough review of the numerous achievements from the GRACE mission can be found in Tapley *et al.* (2019). Additionally, recent efforts to estimate trends from GRACE and GRACE-FO level 1B data directly have allowed the study of trends with even higher resolution (Loomis *et al.* 2021). On the other hand, GRACE data have also been used in high-frequency or short-timescale analyses such as the analysis of storm-induced ocean mass variability (Ghobadi-Far *et al.* 2022), or rapid TWS increases due to flooding (Han *et al.* 2021).

To derive GRACE based gravity solutions, however, background model information is usually required to account for the inherent insensitivity to high frequency mass changes both in the spatial and temporal domains. The GRACE satellites orbit at very low altitudes (less than 500 km) by passing over the North and South Pole every 90 min while the Earth is spinning underneath the orbital plane. This configuration allows dense temporal sampling at the poles, but increasingly sparse coverage towards the equator, so that very rapid mass variations are undersampled at lower latitudes. This includes submonthly mass variations from a variety of sources but most prominently ocean tides with prominent periodicities at diurnal and semi-diurnal frequencies (Ray *et al.* 2003; Han *et al.* 2004; Sulzbach *et al.* 2021), as well as non-tidal variability in atmosphere and ocean, which are conventionally subtracted from the satellite data to mitigate temporal aliasing effects. The Atmosphere and Ocean De-Aliasing Level-1B (AOD1B) product provides this *a priori* background information of atmospheric and oceanic non-tidal mass variations. It is routinely provided by Deutsches GeoforschungsZentrum (GFZ) since the launch of the original GRACE mission in the year 2002 (e.g. Flechtner *et al.* 2006). The recently published new release RL07 of AOD1B (Shihora *et al.* 2022a) improves over previous versions by including new atmospheric data sets and an updated ocean model configuration, which allow for a more accurate representation of the high-frequency non-tidal mass variations on the Earth (Shihora *et al.* 2022b).

However, especially in light of the above cited scientific applications of the final gravity data, AOD1B is not only required to accurately represent the high-frequency mass variations but also feature stability and consistency over long timescales from months

to decades. Large spurious trends, low-frequency signals or bias-jumps in the background data could be erroneously introduced into the final gravity solutions where they are subsequently interpreted in an entirely different geophysical context. Especially over the continents, such trends might be interpreted in the context of TWS changes or ice-mass changes and have a significant impact on the applicability of the final results from the GRACE and GRACE-FO missions.

We here present an analysis of both the trends and annual signal as included in AOD1B RL07 (Section 3 and 4) as well as possible bias jumps by studying 3-hourly tendencies (Section 5). In both cases, we present results separately for the atmospheric as well as the oceanic component of AOD1B and compare to alternative re-analyses as well as the previous release RL06. We also compare both releases in terms of difference in variability in Section 6 before concluding in Section 7 with a summary of the results in the context of the geophysical applications of satellite gravimetry.

2 OVERVIEW OF AOD1B RL07

AOD1B RL07 (Shihora *et al.* 2022b) is based on atmospheric data from atmospheric re-analyses of the European Centre for Medium-range Weather Forecasts (ECMWF) in combination with ocean bottom pressure fields from an ocean general circulation model. The early years of the atmospheric component until 2017 are based on ECMWF's ERA5 re-analysis (Hersbach *et al.* 2020), while from 2018 onwards operational ECMWF data is used to allow for a near-real-time continuation of the data product. To ensure consistency between the two sources, surface pressure fields are mapped to a common reference orography (Dobslaw 2016). In addition to surface pressure variations, density anomalies from the upper atmosphere are considered for the entire time-series as well.

The oceanic component of RL07 is based on ocean bottom pressure (OBP) anomalies specifically simulated for AOD1B with the Max-Planck-Institute for Meteorology Ocean Model (MPIOM; Jungclaus *et al.* 2013), which is consistently forced with atmospheric data from ERA5 until 2017 and ECMWF operational data from 2018 onwards.

Tidal signals in the atmospheric surface pressure as well as corresponding induced signals in the OBP data are empirically estimated and subtracted (Balidakis *et al.* 2022) in order to only represent non-tidal mass-variations. Anomalies are computed with respect to the long-term mean from 2007 to 2014 and are subsequently provided as coefficients of a spherical harmonic expansion up to degree and order (d/o) 180 with a temporal resolution of 3 hr. RL07 is being produced starting in the year 1975, which coincides with the launch of the Starlette satellite, to allow for the consistent processing of even the earliest satellite laser ranging (SLR) data. AOD1B RL07 is publicly available under Shihora *et al.* 2022a while more details on initial geodetic validation are provided in Shihora *et al.* (2022b).

3 ASSESSMENT OF LINEAR TRENDS

As a first step, we analyse the trends in the components of AOD1B RL07 in order to assess their possible impact on the estimated GRACE gravity field time series. The analysis is split into the individual components of AOD1B, that is (i) the atmospheric surface pressure, (ii) contributions from density anomalies in the upper atmosphere and (iii) ocean bottom pressure.

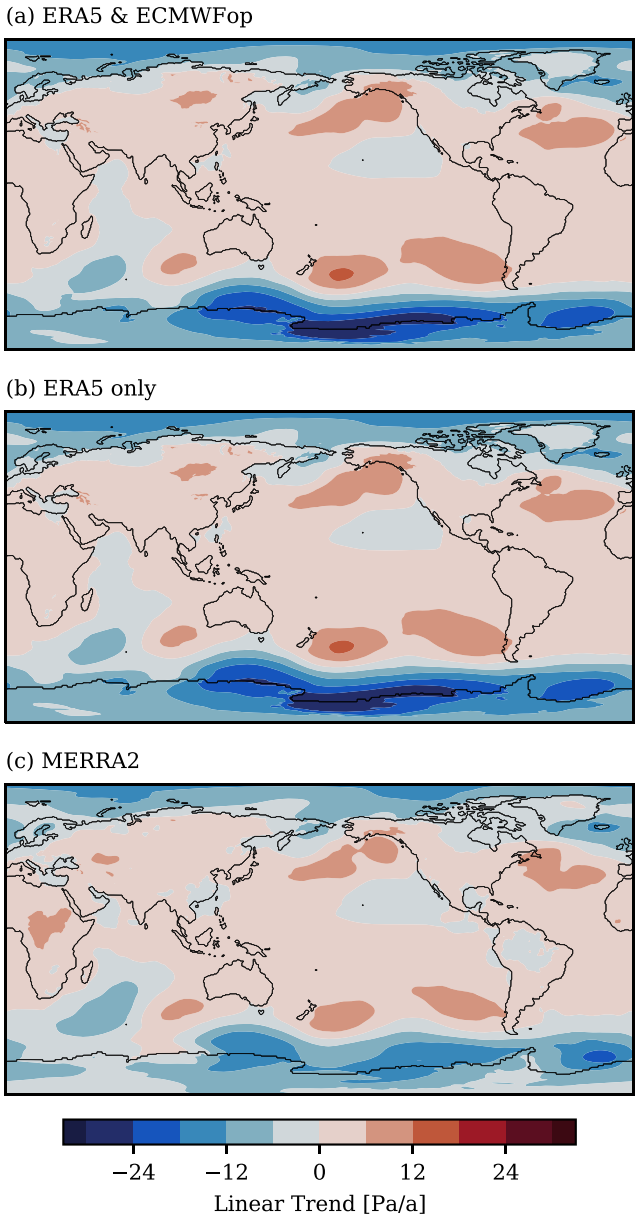

Figure 1. Linear trends in surface pressure as it is used for AOD1B RL07 as a combination of ERA5 (2002–2017) and ECMWF operational data (2018–2020) (a). As a reference (b) and (c) show the linear trends in surface pressure when considering only ERA5 re-analysis data or the MERRA2 re-analysis. All trends are computed from 2002 to 2020.

3.1 Surface pressure

Fig. 1 shows the linear trend for the atmospheric surface pressure as it is included in AOD1B RL07 in subfigure (a). It consists of data from the ERA5 re-analysis until 2017 followed by ECMWF operational data starting in 2018. To ensure that there is no impact due to the transition between the two data sets we also show the trend when using only the ERA5 re-analysis (b) as well as surface pressure from the MERRA2 re-analysis (Gelaro *et al.* 2017) as a reference (c). The trends are computed starting in January 2002 shortly before the launch of GRACE until the end of the year 2020.

We conclude that the surface pressure contribution to AOD1B RL07 does not include large trends. The largest local signals are found along the coast of Antarctica and in the Ross Sea with values

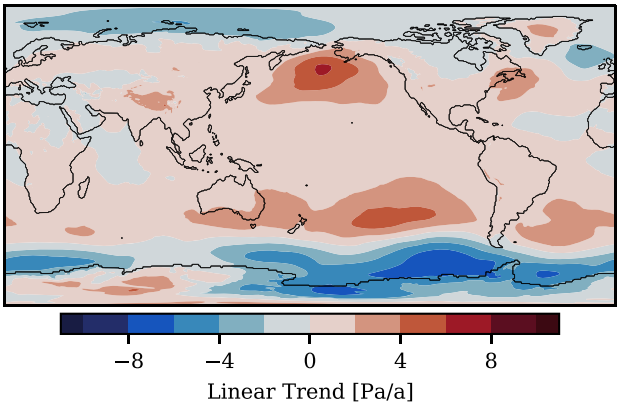

Figure 2. Linear trend of ERA5 surface pressure from 1975 to 2020.

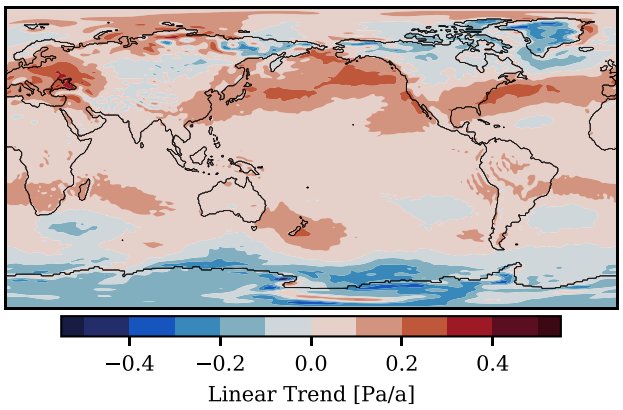

Figure 3. Linear trend of the upper-air density anomalies from 2002 to 2020 as included in AOD1B RL07.

of up to 30 Pa a^{-1}. Over the continents values are even smaller reaching only up to 5 Pa a^{-1}. Trends using the combination of ERA5 and ECMWF operational data (Fig. 1a) are very close to the results obtained from using only the ERA5 re-analysis (Fig. 1b) indicating that the transition between the data-sets does not have a significant effect. Surface pressure trends over the period from 2002 to 2020 from MERRA2 (Fig. 1c) show a very similar pattern to the other results. The largest trends are also found in the southern ocean close to Antarctica, although the trends are, with values of up to 15 Pa a^{-1}, slightly smaller.

Since AOD1B RL07 is produced all the way back to the year 1975, we also compute the linear trend over a longer time period in Fig. 2. The figure shows the linear trend in ERA5 surface pressure for 1975 until 2020. For this period, trends are globally below 8 Pa a^{-1} and significantly below 5 Pa/a over the continents with a global average of 0.47 Pa a^{-1}. Comparing the trends on longer timescales to the results from Fig. 1 the feature along the coast of Antarctica is much reduced, indicating that the pattern is not related to long-term drifts but rather to interannual-to-decadal climate variability. In view of the strong variability in surface pressure in the area and the importance of atmosphere–ocean interactions on the long-term evolution of the regional atmospheric circulation, such a trend in the region is indeed plausible. However, the representation of surface pressure signals around Antarctica is likely less accurate due to a sparser coverage of assimilated observational data. Part of this can be seen from the difference in trend between ERA5 and MERRA2. This also matches Hobbs *et al.* (2020) who report that the exact distribution and magnitude of long-term pressure changes around Antarctica varies in different re-analysis data-sets. These uncertainties in the atmospheric data should thus be considered for a new assessment of the remaining uncertainty of AOD1B RL07 that is currently under preparation.

3.2 Upper air density anomalies

In addition to surface pressure anomalies, AOD1B RL07 takes the contribution of upper air density anomalies (Swenson & Wahr 2002) over both continents and oceans into account. To visualize the effects in an accessible way, we transform the upper air gravitational effects into apparent surface pressure variations that would have caused the same effect on the gravity field outside the atmosphere for the trend assessment presented here.

Fig. 3 shows the linear trend in the contribution of upper-air density anomalies computed for the years 2002–2020. Trends are much smaller compared to contributions from atmospheric surface pressure due to the comparatively small deviations from the hydrostatic balance. Regionally, those trends do not exceed 0.5 Pa a^{-1}, and for most of the grid points values are even much smaller. On a area-weighted global average, the linear trend amounts to about 0.05 Pa a^{-1} which is well within the expected range of natural climate variability and will thus not introduce any artificial trends into AOD1B.

3.3 Ocean bottom pressure

Ocean bottom pressure forms the third major component of the non-tidal mass variability represented by AOD1B. Transient simulations with MPIOM and forcing from either ERA5 or the operational ECMWF data are used to calculate OBP fields every 3 hr. Especially for oceanic applications of satellite gravimetry, large secular trends in the simulated OBP can also significantly reduce the quality of the gravity field solutions, since monitoring the long-term increase in ocean mass is one of the most important science goals of satellite gravimetry in maritime regions (Chambers *et al.* 2010).

In Fig. 4(a), we present the trend in OBP as it is used in AOD1B RL07 based on ERA5 atmospheric forcing until 2017 and operational ECMWF forcing data from 2018. Similar to Section 3.1, we also compare to OBP trends using only ERA5 atmospheric forcing in the MPIOM simulation (b) in order to gauge the impact of changed forcing data. Additionally, we compare the trends to the previous release 06 of AOD1B (c) (Dobslaw *et al.* 2017). Similar as before, all three trends are computed over the period 2002–2020.

Trends in the oceanic component of AOD1B (Fig. 4a) are regionally around 20 Pa a^{-1}. The largest trends are found in the south in the region of the Antarctic Circumpolar Current (ACC), especially in the Bellingshausen Basin. This region experiences some of the highest speeds on Earth, and signals in Fig. 4 reflect an adjustment of the ocean dynamics to the atmospheric forcing in a region where the shape of the ocean's bathymetry favours resonant ocean mass redistribution. Additionally, shallow parts of Arctic Ocean show trends of similar magnitude but opposite sign. On a global average, the absolute magnitude of linear trends is below 7 Pa a^{-1}.

Comparisons with OBP trends based on ERA5 atmospheric forcing only (Fig. 4b) reveals very little impact from the transition in forcing data. Both regional patterns as well as the magnitudes of trends are highly similar. Trends in the previous release 06 of AOD1B are generally comparable in magnitude, but show a different regional pattern. Whereas the trends in the Arctic Ocean are largely the same, trends in the Southern Ocean are not as clearly

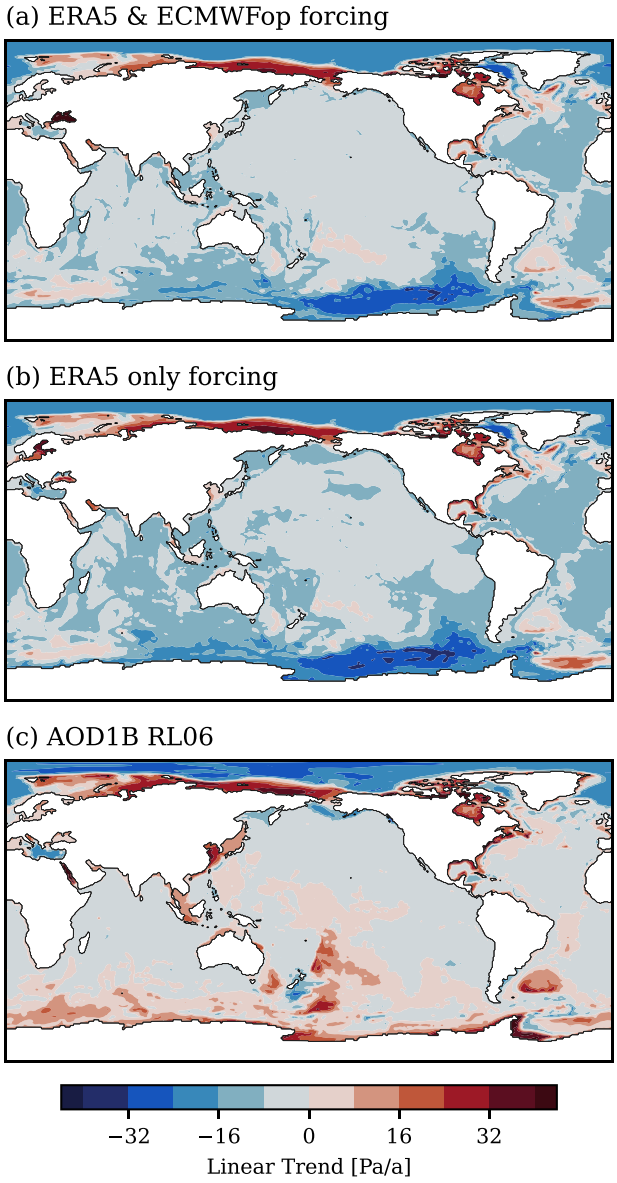

Figure 4. Linear trends in the ocean bottom pressure contribution as included in AOD1B RL07 (a) where both ERA5 and ECMWF operational atmospheric forcing data are used. Panel (b) shows the linear trend when only using ERA5 atmospheric forcing data. Panel (c) shows the linear trend from AOD1B RL06 for comparison. All trends are computed from 2002 until 2020.

defined. Instead, there are smaller regions with locally increased trends. We attribute these patterns primarily to an insufficient spin-up of the ocean simulation, which has been extended to 2.000 years for RL07, and also to the consequences of the higher quality of the (more recent) atmospheric re-analysis data utilized for RL07.

We also compute the linear trend in ocean bottom pressure over a longer period from 1975 until 2020 in Fig. 5. Whereas the spatial pattern in the Southern Ocean is very similar to results in Fig. 4(a), the overall magnitude of the trend is reduced. Trends in coastal areas and the Arctic Ocean are also significantly smaller. We therefore conclude that the trends in OBP, which are of a comparable amplitude to surface pressure trends, are at an acceptable level of

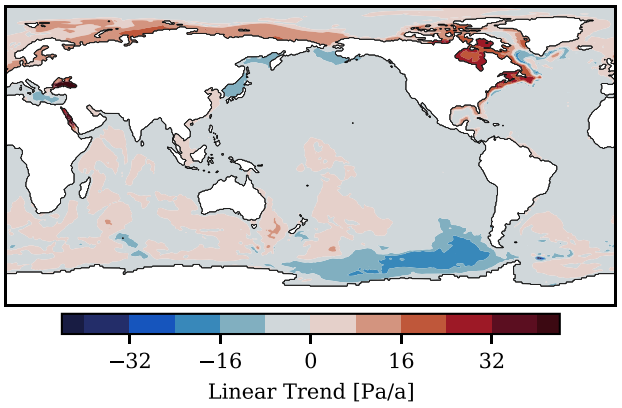

Figure 5. Linear trend of MPIOMs ocean bottom pressure from 1975 to 2020.

accuracy in AOD1B RL07, but a tiny contribution of artificial drift from the ocean model might still enter the gravity fields.

For comparison, Rodell *et al.* (2018) estimate the uncertainty of the GRACE-based TWS trend for Antarctica to be ∼40 Gt a^{-1} which corresponds to about 0.3 cm a^{-1} equivalent water-height which is still larger than the ERA5-based trend signal over the Antarctic region. Similarly, the uncertainty of global ocean mass change as estimated by GRACE is given by Tapley *et al.* (2019) to be ∼0.4 mm a^{-1} which is on the same order of magnitude as the globally averaged OBP trends in AOD1B RL07. Please note that although Chen *et al.* (2022) give estimates on the order of ±0.05 mm a^{-1}, this number is based on the misfit of the GRACE data in the linear regression and does not include uncertainties based on, for example GIA and geocentre motion which have additional impacts of approximately ±0.3 mm a^{-1} (Chambers *et al.* 2010) or approximately ±0.21 mm a^{-1} (Blazquez *et al.* 2018), respectively.

Whereas the drift remaining in AOD1B RL07 is acceptable at the current level of GRACE-based trends, further efforts are certainly needed in case that a future gravity mission of the next generation is being implemented, which probably shall provide more accurate gravity field data from better instruments, more satellites, and lower orbit altitudes as well as extend the time-series of gravity solutions. In addition, care must be taken in handling background model information when it comes to the computation of GRACE-based trends, as the residual drift in AOD1B is now on the order of magnitude of GRACE trend uncertainties.

4 ASSESSMENT OF THE ANNUAL SIGNAL

Next to long-term linear trends, the accuracy of low frequency signals such as annual variations is of interest. In principle, these long term signals do not contribute to the temporal aliasing in the gravity field solutions. As satellite gravimetry is, however, inherently incapable of distinguishing between individual vertical contributions to mass variations, background models are often applied also for signal separation. In the analysis of TWS data for instance, atmospheric mass variations must be removed by subtracting the variations as represented by AOD1B. As a result, a proper representation of longer frequencies such as the annual signal can be important in many applications of the gravity data.

In Fig. 6, we show the amplitude of the annual variations in surface pressure based on ERA5 (Fig. 6a) and MERRA2 (Fig. 6b) data from 2002 to 2020.

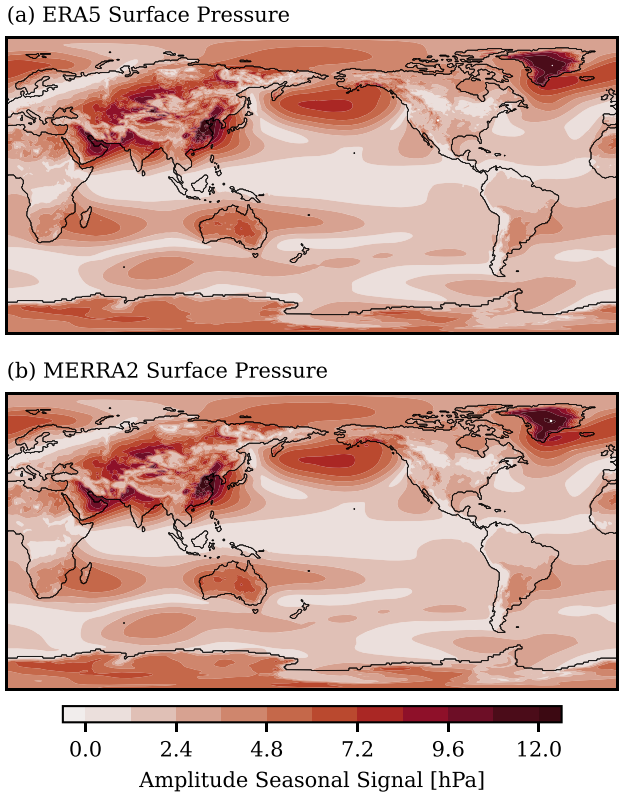

Figure 6. Amplitude of the seasonal signal from ERA5 (a) and MERRA2 (b) surface pressure estimated from 2002 to 2020.

The signal is largest over Greenland, where amplitudes of over 12 hPa are reached. Similarly large signals can be found in some coastal areas such as the East China Sea or the Persian Gulf. Over most of the ocean, however, the amplitude is typically below 1 hPa. Comparing the amplitudes from the two re-analyses shows a very small difference. Most of the differences are found in regions with steep orographic gradients which might be the cause of some of these differences as we did no adjustment to a common orography. The spatially averaged absolute value of the difference reaches only 11 Pa which, given the magnitude of the annual signal, is negligible. The small discrepancy can be attributed to the large weight of the identical barometer observations in both re-analyses.

5 ASSESSMENT OF 3-HOURLY TENDENCIES

So far, the assessment of the individual components of AOD1B RL07 has focused only on the stability on decadal timescales. However, errors on short timescales such as bias changes, can have an equally adverse impact on GRACE gravity field solutions (Fagiolini *et al.* 2015). In this section, we examine 3-hourly tendencies which are an effective statistical metric to reveal abrupt jumps or other subtle discontinuities in the underlying data. 3-hourly tendencies are here defined as the differences between consecutive 3-hourly time-steps and are thus a measure of the amount of change from one data epoch to the next. A sudden large peak in the tendencies would be an indicator of a bias jump, which would require further scrutiny. We focus here again on the individual components of RL07, namely the atmospheric component which combines the surface pressure anomalies and the upper air density contributions, as well as the

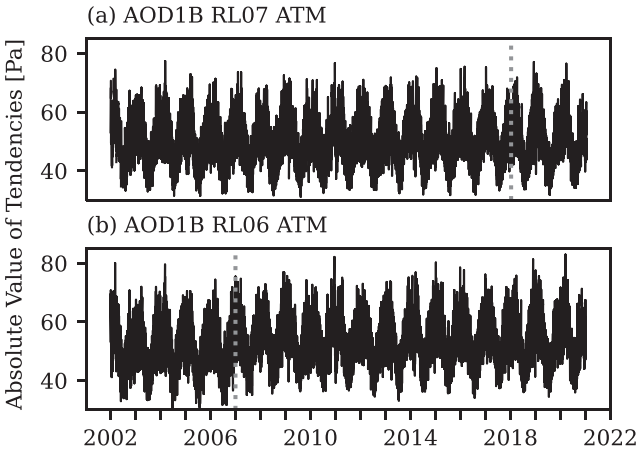

Figure 7. Area-weighted spatial mean of the absolute value of 3-hourly tendencies for the atmospheric component of AOD1B. Results are shown for RL07 (a) and RL06 (b). The transition from re-analysis data to operational ECMWF data is indicated by the vertical dotted lines.

oceanic component. We place a special focus on the transition between the ERA5 and operational ECMWF atmospheric data as this marks a significant change within the time-series where ensuring consistency is particularly important since it coincides with the gap between the two missions GRACE and GRACE-FO.

5.1 Atmospheric component

First, we consider the tendencies of the atmospheric contribution to RL07. In Fig. 7, we show the 3-hourly tendencies as a single time-series by computing the area-weighted mean of the absolute value of the tendencies. The time-series is shown for RL07 (a) as well as RL06 (b) for comparison. The dotted vertical line marks the epoch of transition from re-analysis to the operational ECMWF atmospheric data in the respective release (i.e. 1 January 2007 in RL06, and 1 January 2018 in RL07).

The atmospheric tendencies for RL07 are largely comparable to the corresponding results from RL06. Both the overall magnitude of the tendencies as well as the scatter of the intra-annual variations agree well as shown in Fig. 7. In addition, there is no evidence for trends or significant peaks visible which would indicate a bias jump in the atmospheric data. While RL06 shows a slight increase in the tendencies after 2007 due to the change in spatial resolution after the transition from ERA-Interim to operational ECMWF data, the impact of the transition for RL07 in 2018 is even smaller.

5.2 Oceanic component

Next, we consider the tendencies for the oceanic component of AOD1B RL07. Similar to the previous section we compute the area-weighted absolute value of the tendencies to arrive at time-series for both RL06 and RL07 as shown in Fig. 8. Both tendency time-series are comparable in terms of seasonal variation, however, the RL07 results show overall slightly larger values. In addition, there is a change in the tendencies visible over the transition from re-analysis to operational atmospheric forcing data. In RL07, we note a decrease in the tendencies after 2018, whereas for RL06 the oceanic tendencies increase after 2007. For RL06 the change from ERA-Interim to operational ECMWF data included a notable change in spatial resolution and as a result shows a slight impact on the variability in the MPIOM simulation. The change in RL07 is rather

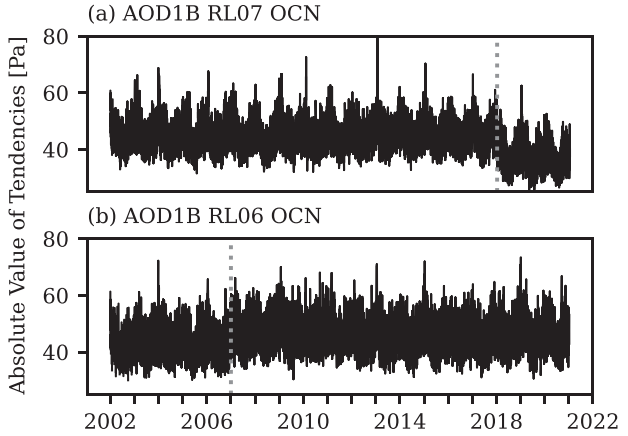

Figure 8. Area-weighted spatial mean of the absolute value of 3-hourly tendencies for the oceanic component of AOD1B. Results are shown for RL07 (a) and RL06 (b). The transition in atmospheric forcing data from re-analysis to operational ECMWF data is indicated by the vertical dotted lines.

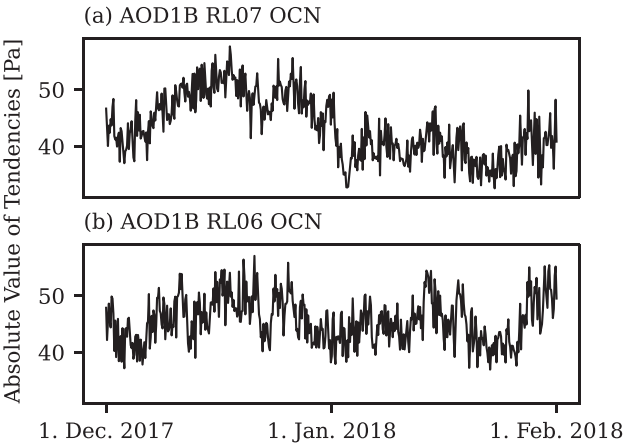

Figure 9. Area-weighted spatial mean of the absolute value of 3-hourly tendencies for the oceanic component of AOD1B for the transition from 2017 to 2018 which signifies the transition in the atmospheric forcing data. Results are shown for RL07 (a) and RL06 (b).

due to the different atmospheric forcing frequency in the simulation. As RL07 aims to take full advantage of the newly increased 1-hourly resolution of the ERA5 re-analysis, the transition to operational data also includes a reduction in the forcing frequency of MPIOM to 3-hourly sampled forcing fields. As a result, a decrease in the variability from each time-step to the next is found, since advected atmospheric fronts are less sharply defined with fewer time-steps. The sensitivity to the change in atmospheric forcing thus shows that the tendencies can indeed identify even very subtle changes in the underlying data.

We also show the tendencies for a much shorter period around the transition in forcing data in Fig. 9 to ensure that there are indeed no abrupt changes. The figure shows the tendencies for two months around the transition to operational forcing for the oceanic part of RL07. As a reference we also show the tendencies over the same period for RL06 which does not include any change in atmospheric data during that time. The comparison between the two time-series reveals no conspicuous features. While the tendencies decrease, they do so rather smoothly and well within the usual range of the otherwise typical variability.

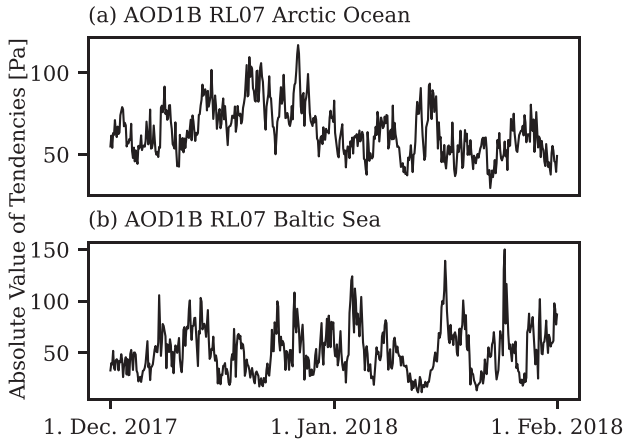

Figure 10. Area-weighted spatial mean of the absolute value of 3-hourly tendencies for the oceanic component of AOD1B RL07 for the transition from 2017 to 2018 which signifies the transition in the atmospheric forcing data. Tendencies are computed using only the arctic ocean (a) or the Baltic sea (b).

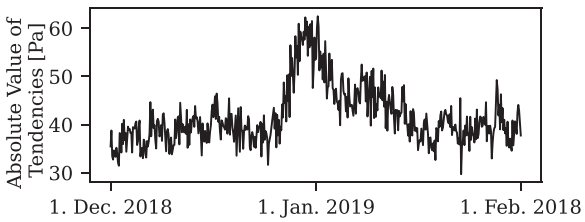

Figure 11. Area-weighted spatial mean of the absolute value of 3-hourly tendencies for the oceanic component of AOD1B RL07 from December 2018 to February 2019.

As the analysis has so far focused on the consistency on a global scale, we now also analyse the impact of the forcing transition in two key regions of the world. Fig. 10(a) shows the tendencies around the transition epoch for the Arctic Ocean, which is usually under-represented in the global average analysis due to its rather small total area but features a comparatively high variability in OBP. In Fig. 10(b), we show tendencies for the Baltic Sea, which is a semi-enclosed sea and thereby challenging to model given the spatial resolution of MPIOM. Whereas the tendencies for those two regions show a larger amount of variability than the global average, there is no indication of an adverse impact of the transition in atmospheric forcing data even on those regional scales.

A second notable feature of the tendencies shown in Fig. 8(a) are small peaks that appear at irregular intervals in some years. Those peaks are visible at the same times also in the tendencies calculated from RL06. As they appear in two separate time-series that are based on both different ocean model configurations and different atmospheric forcing data-sets, they are likely a physical feature in the simulation rather than a bias jump. To verify, we first show a detailed view of the tendencies for one of the peaks in Fig. 11. The figure shows that the increase in tendencies is not due to a single time-step, which would indicate a bias jump, but instead stretches for about 1 week around the end of December 2018. As the time-series shown in Fig. 11 is based on a spatial average, we also determine the spatial distribution of the increased tendencies. We average the absolute value of the tendencies for the week of increased tendencies and subsequently subtract a long-term mean. The difference is shown in Fig. 12. Regions that contribute

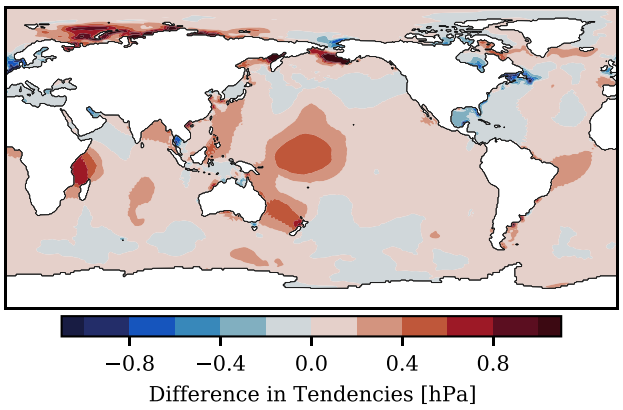

Figure 12. Spatial distribution of the increased tendencies for the last week of December 2018. Tendencies are averaged over 1 week around the increase in the tendencies and a long term mean is subsequently subtracted.

to the temporary increase in tendencies are thus shown as spatially coherent positive signals. Based on the figure we can identify three core regions which have the largest contributions: the Mozambique Channel, the Tasman Sea and the western equatorial Pacific. All three of these regions are, due to their basin-geometry, resonant at very short periods extending over a few hours. This can be readily seen for example from the spatial distribution of semi-diurnal ocean tides (Sulzbach *et al.* 2021). While other regions in Fig. 12 also show a positive difference, such as the Arctic or the North Sea, a close inspection of the time-series of these regions shows that they do not contribute to the temporary increase in variability. These regions, instead, have a generally larger variability and thus happen to feature in the figure. Based on the assessments of Figs 11 and 12, we conclude that the increase in variability is not due to a change in bias or a technical issue but rather caused by occasionally happening resonances in certain oceanic regions.

5.3 ERA5 back extension

As AOD1B RL07 is starting in 1975, the first four years are based on the so-called back extension of the ERA5 re-analysis (Bell *et al.* 2021) which covers the years from 1950 to 1978. To assess the transition between the back extension and the regular ERA5 data, we also compute tendencies for the components of AOD1B RL07 across the transition. Fig. 13 shows the area-weighted absolute value of the tendencies for both the atmosphere (Fig. 13a) as well as the oceanic component (Fig. 13b) from 1978 to 1979.

The 3-hourly tendencies clearly show an impact of the change from back extension to the regular ERA5 data both for the atmosphere as well as the simulated ocean bottom pressure data forced with the atmospheric data. For the atmosphere, the back extension based data exhibit a significantly larger variation in the tendencies. Bell *et al.* (2021) report a significant improvement in the quality of the surface pressure data beginning in 1979 coinciding with the introduction of the TIROS Operational Vertical Sounder (TVOS) satellite data (see Bell *et al.* 2021, fig. 9). A corresponding change is visible in the oceanic tendencies as well. Both the variation as well as the overall magnitude of the 3-hourly tendencies changes across the transition.

While the impact is not overly large, there is thus a change in the highest frequencies of AOD1B RL07 for the earliest years. We believe that this will not significantly impact applications such as the processing of the earliest SLR satellites as the accuracy of the early

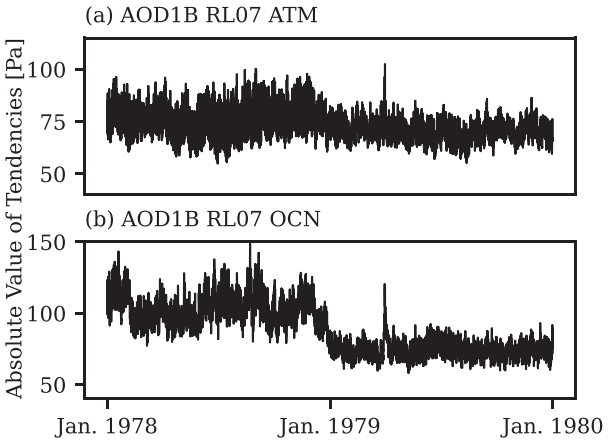

Figure 13. Area-weighted spatial mean of the absolute value of 3-hourly tendencies. Results are given for surface pressure (a) as well as AOD1Bs oceanic component (b) for 1978–1979. The period covers the transition from the back extension to regular ERA5 re-analysis data.

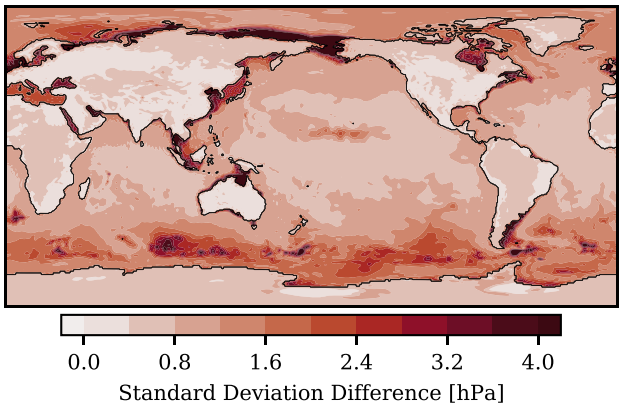

Figure 14. Standard deviation of the difference between AOD1B RL07 and RL06 GLO coefficients after retransformation from spherical harmonic coefficients.

SLR tracking data is significantly lower than today. As an example, the assimilation of normal points for the ITRF2020 from the ILRS starts in 1983 (Noll *et al.* 2019) only, which is in part driven by the reduced accuracy of instruments as well as a poorer coverage of ground stations. Nonetheless, the impact of the lower accuracy of the ERA5 Back Extension based years in AOD1B should be kept in mind when using the years 1975–1979.

6 COMPARISON TO AOD1B RL06

We finally assess the overall impact of the various changes in AOD1B RL07 on the surface mass variability in general. To that end, we compare the so called GLO coefficients—which combine the effects of atmosphere and ocean and are routinely applied during the GRACE gravity field processing—from RL06 and RL07. In Fig. 14, we show the standard deviation difference between the GLO coefficients that have been re-synthesized from the Stokes Coefficients into the spatial domain.

The difference in variability between RL07 and RL06 generally reach an amplitude of about 4 hPa on regional scales. Especially in the Southern Ocean and the region of the ACC as well as several coastal areas. In contrast, the differences over the continents are

significantly smaller and are well below 1 hPa. Generally, the differences in the atmospheric contribution between RL07 and RL06 are much smaller than in the oceanic component. This is largely due to the common code base of the ERA5 and ERA-Interim reanalyses which are the basis of the RL07 and RL06 atmospheric components, respectively. The oceanic component, as it is based on unconstrained ocean simulations, has undergone more significant changes such as the inclusion of the feedback of self-attraction and loading to the ocean dynamics (Shihora *et al.* 2021). In combination with the change to the ERA5 re-analysis as atmospheric forcing data which offers higher spatial and temporal resolutions, this changes the OBP signals as shown in the previous Section. Together with differences due to intrinsic variability which are prominent in the Southern Ocean (Zhao *et al.* 2021), and the lack of observational constraints, larger differences in the oceanic components between RL07 and RL06 are the consequence.

Whereas validation of the previous RL06 of AOD1B with altimetry (Bonin & Save 2020) and experimental daily GRACE solutions (Schindelegger *et al.* 2021) have indicated deficiencies especially for the ocean component of AOD1B, we are confident that differences between RL06 and RL07 as visible in Fig. 14 reflect in particular improvements in the high frequency mass variations as evidenced by Shihora *et al.* (2022b). This, however, raises the question of how large the remaining uncertainties are, so that residual errors in background modelling can be properly incorporated into the stochastic modelling of the GRACE gravity field processing. The latest thorough error assessment for AOD1B is based on AOD1B RL05 (Dobslaw *et al.* 2016), which was vetted as applicable to RL06 within a subsequent simulation study (Poropat *et al.* 2020). Differences found between RL06 and RL07 suggest, however, that this assessment is no longer representative and needs to be revisited. This is especially important, as the inclusion of background model uncertainties has been shown to have a positive impact on the gravity field estimation process (Zenner *et al.* 2010; Kvas *et al.* 2019) and in dedicated mission performance simulation studies (Abrykosov *et al.* 2022).

7 CONCLUSIONS

Release 07 of the Atmosphere and Ocean de-aliasing Level-1B product available in terms of 3-hourly sampled sets of Stokes Coefficients expanded up to degree and order 180 has been thoroughly assessed in this study for the whole period between 1975 and 2021. Both long-term trends as well as short term inconsistencies such as bias jumps that might have a significant impact on the GRACE gravity field solutions have been examined.

In Section 3 we have focused on identifying and quantifying potential long-term trends in all three components of AOD1B: the atmospheric surface pressure anomalies, contributions from density anomalies in the atmosphere and ocean bottom pressure anomalies. For all three components we conclude that the existing trends are at an acceptable level for the inclusion in AOD1B RL07. The largest contribution to the linear trend, when computed over a 40-yr timespan, comes from the oceanic component where trends still do not exceed 30 Pa a^{-1}. Trends over the same period for the atmospheric contributions are much smaller. GRACE-based trends, such as analysed by Loomis *et al.* (2021) or TWS based trend as published by Rodell *et al.* (2018), are generally on the order of 1 cm a^{-1} which is equivalent to 1 hPa a^{-1}. The uncertainties of the trends are, as an example, estimated to be on the order of 30 Pa a^{-1} equivalent water-height for ice-mass loss in Antarctica and thus still larger that the trends included in AOD1B RL07. Atmospheric trends in AOD1B RL07 are also comparable to previous releases and current state-of-the-art re-analysis data which, due to their observational basis, do not include large artificial trends. For the ocean, the trends are acceptable given the current accuracy of satellite gravimetry based trend analyses. For future gravity missions, however, efforts should be made to further reduce the remaining drift.

To assess the consistency over short time-scales we have computed 3-hourly tendencies for the atmospheric and oceanic contributions separately. These tendencies are defined as differences between consecutive 3-hourly time-steps. The change in the atmospheric forcing of the ocean simulation from re-analysis data to operational ECMWF data can be identified in the tendencies, showing that they are indeed a sensitive diagnostic to identify possible issues. They have also been used for the assessment of previous releases of AOD1B and have helped to identify possible model changes such as changes in the integrated forecast system of the operational ECMWF atmospheric data which might include changes in the resolution. As they are also an easily computed quantity, tendencies make a useful tool for the assessment of other model-based data sets both during preparation as well as during operational production. At GFZ, this includes effective angular momentum functions (Dobslaw *et al.* 2010) and non-tidal loading grids (Dill & Dobslaw 2013) which are produced from data sources similar to AOD1B.

A closer examination of the transition in atmospheric forcing in the ocean simulation shows that there are no inconsistencies or bias jumps induced by the change. This is found to be true also for rather sensitive areas of the ocean domain such as the Arctic Ocean or the Baltic Sea.

An additional assessment of the impact of the ERA5 Back Extension, which is used for the years 1975–1978 of AOD1B RL07, shows that there is indeed a difference in the variability of atmospheric surface pressure and thus also simulated ocean bottom pressure. Although this will likely not negatively affect the processing of, for example the earliest SLR satellite data, these differences should be kept in mind when using the earliest years of AOD1B. In summary, there is no indication of unexpected behaviour that could negatively affect the application of the background model data in either the oceanic or atmospheric component of AOD1B RL07 especially for the application in satellite gravimetry from GRACE and GRACE-FO.

Atmospheric and oceanic background models are not only applied in the processing of satellite gravimetry but are also applied in, for example altimetry via the Dynamic Atmospheric Corrections (DAC) product (Carrère & Lyard 2003; Carrère *et al.* 2016). Also for these background models, tendencies can be a valuable tool for the routine assessment of the consistency of the data due to their sensitivity to model changes or inconsistencies and their straightforward computation.

Finally, we have assessed the differences in the mass variations of RL06 and RL07. We find that the largest differences are found in the ocean domain, which is to be expected given then more significant changes in the ocean model configuration for RL07. As analyses of RL07 indicate a globally improved representation of the mass-variations with respect to RL06, we conclude that previous studies on the uncertainties of AOD1B (Dobslaw *et al.* 2016; Poropat *et al.* 2020) are not sufficiently applicable to RL07 and need to be revisited. We thus propose a new quantification of the remaining uncertainties in AOD1B, especially in the oceanic domain due to the lack of observational constraints. We believe that such a new assessment, including uncertainties due to differences between state-of-the-art atmospheric re-analyses as well as the impact of the

atmospheric forcing and the initial conditions of the ocean simulation, can have a significant impact on the quality of the final gravity field solutions from satellite gravimetry.

ACKNOWLEDGMENTS

This work has been supported by the German Research Foundation (grant no. DO 1311/4-1) as part of the research group NEROGRAV (FOR 2736). Production of AOD1B RL07 is supported by the ESA contract No. 4000135530. KB is funded by the DFG via the Collaborative Research Cluster TerraQ (SFB 1464, Project-ID 434617780). Deutscher Wetterdienst (Offenbach, Germany) and the European Centre for Medium-range Weather Forecasts (Reading, U.K.) are acknowledged for granting access to ECMWF operational data. Numerical analyses were performed at Deutsches Klimarechenzentrum (DKRZ) in Hamburg (Germany) under Project-ID 0499. Calculations carried out herein were facilitated by using the Climate Data Operators software suite (Schulzweida 2022).

DATA AVAILABILITY STATEMENT

AOD1B RL07 is publicly available via Shihora *et al.* (2022a). RL06 data can be accessed through GFZs Information System and Data Center under https://isdc.gfz-potsdam.de/ as well. Access to the ECMWF ERA5 re-analysis is provided via the Climate Data Store https://cds.climate.copernicus.eu (Hersbach *et al.* 2020). The MERRA2 re-analysis (Gelaro *et al.* 2017) can be found at the Goddard Earth Sciences Data and Information Services Center under https://disc.gsfc.nasa.gov/datasets?project=MERRA-2.

REFERENCES

Abrykosov, P., Sulzbach, R., Pail, R., Dobslaw, H. & Thomas, M., 2022. Treatment of ocean tide background model errors in the context of GRACE/GRACE-FO data processing, *Geophys. J. Int.,* **228**(3), 1850–1865.

Balidakis, K., Sulzbach, R., Shihora, L., Dahle, C., Dill, R. & Dobslaw, H., 2022. Atmospheric contributions to global ocean tides for satellite gravimetry, *J. Adv. Model. Earth Syst.,* **14**(11), doi:10.1029/2022MS003193.

Bell, B., *et al.*, 2021. The ERA5 global reanalysis: preliminary extension to 1950, *Q.J.R. Meteorol. Soc.,* **147,** 4186–4227.

Blazquez, A., Meyssignac, B., Lemoine, J.M., Berthier, E., Ribes, A. & Cazenave, A., 2018. Exploring the uncertainty in GRACE estimates of the mass redistributions at the Earth surface: implications for the global water and sea level budgets, *Geophys. J. Int.,* **215**(1), 415–430.

Bonin, J. A. & Save, H., 2020. Evaluation of sub-monthly oceanographic signal in GRACE "daily" swath series using altimetry, *Ocean Sci.,* **16**(2), 423–434.

Carrère, L. & Lyard, F., 2003. Modeling the barotropic response of the global ocean to atmospheric wind and pressure forcing - comparisons with observations, *Geophys. Res. Lett.,* **30**(6), doi:10.1029/2002GL016473.

Carrère, L., Faugère, Y. & Ablain, M., 2016. Major improvement of altimetry sea level estimations using pressure-derived corrections based on ERA-Interim atmospheric reanalysis, *Ocean Sci.,* **12**(3), 825–842.

Chambers, D. P., Wahr, J., Tamisiea, M. E. & Nerem, R. S., 2010. Ocean mass from GRACE and glacial isostatic adjustment, *J. geophys. Res.,* **115**(B11), doi:10.1029/2010JB007530.

Chen, J., Tapley, B., Save, H., Tamisiea, M.E., Bettadpur, S. & Ries, J., 2018. Quantification of ocean mass change using gravity recovery and climate experiment, satellite altimeter, and argo floats observations, *J. geophys. Res.,* **123,** 10 212–10 225.

Chen, J., Cazenave, A., Dahle, C., Llovel, W., Panet, I., Pfeffer, J. & Moreira, L., 2022. Applications and challenges of GRACE and GRACE follow-on satellite gravimetry, *Surv Geophys,* **43,** 305–345.

Dill, R. & Dobslaw, H., 2013. Numerical simulations of global-scale high-resolution hydrological crustal deformations, *J. geophys. Res.,* **118,** 5008–5017.

Dobslaw, H., 2016. Homogenizing surface pressure time-series from operational numerical weather prediction models for geodetic applications, *J. Geod. Sci.,* **6** , doi:10.1515/jogs-2016-0004.

Dobslaw, H., Dill, R., Grötzsch, A., Brzeziński, A. & Thomas, M., 2010. Seasonal polar motion excitation from numerical models of atmosphere, ocean, and continental hydrosphere, *J. geophys. Res.,* **115**(B10), doi:10.1029/2009JB007127.

Dobslaw, H., *et al.*, 2016. Modeling of present-day atmosphere and ocean non-tidal de-aliasing errors for future gravity mission simulations, *J. Geod.,* **90,** 423–436.

Dobslaw, H., Bergmann-Wolf, I., Dill, R., Poropat, L., Thomas, M., Dahle, C. & Esselborn, S., 2017. A new high-resolution model of non-tidal atmosphere and ocean mass variability for de-aliasing of satellite gravity observations: AOD1B RL06, *Geophys. J. Int.,* **211,** 263–269.

Fagiolini, E., Flechtner, F., Horwath, M. & Dobslaw, H., 2015. Correction of inconsistencies in ECMWF's operational analysis data during de-aliasing of GRACE gravity models, *Geophys. J. Int.,* **202**(3), 2150–2158.

Flechtner, F., Schmidt, R. & Meyer, U., 2006. De-aliasing of short-term atmospheric and oceanic mass variations for GRACE, in *Observation of the Earth System from Space,* pp. 83–98, eds Flury, J., Rummel, R., Reigber, C., Rothacher, M., Boedecker, G. & Schreiber, U., Springer.

Gelaro, R., McCarty, W., Suárez, M.J., Todling, R., Molod, A., Takacs, L. *et al.*, 2017. The modern-era retrospective analysis for research and applications, version 2 (MERRA-2), *J. Climate,* **30**(14), 5419–5454.

Ghobadi-Far, K., *et al.*, 2022. Along-orbit analysis of GRACE follow-on inter-satellite laser ranging measurements for sub-monthly surface Mass variations, *J. geophys. Res.,* **127,** doi:10.1029/2021JB022983.

Han, S.-C., Jekeli, C. & Shum, C. K., 2004. Time-variable aliasing effects of ocean tides, atmosphere, and continental water mass on monthly mean GRACE gravity field, *J. geophys. Res.,* **109**(B4), doi:10.1029/2003JB002501.

Han, S., Yeo, I., Khaki, M., McCullough, C.M., Lee, E. & Sauber, J., 2021. Novel along-track processing of GRACE follow-on laser ranging measurements found abrupt water storage increase and land subsidence during the 2021 March Australian flooding, *Earth Space Sci,* **8** , doi:10.1029/2021EA001941.

Hersbach, H., *et al.*, 2020. The ERA5 global reanalysis, *Q.J.R. Meteorol. Soc.,* **146,** 1999–2049.

Hobbs, W. R., Klekociuk, A. R. & Pan, Y., 2020. Validation of reanalysis Southern Ocean atmosphere trends using sea ice data, *Atmos. Chem. Phys.,* **20,** 14 757–14 768.

Jungclaus, J.H., Fischer, N., Haak, H., Lohmann, K., Marotzke, J., Matei, D., Mikolajewicz, U. *et al.*, 2013. Characteristics of the ocean simulations in the Max Planck Institute Ocean Model (MPIOM) the ocean component of the MPI-Earth system model: MPIOM CMIP5 ocean simulations, *J. Adv. Model. Earth Syst.,* **5,** 422–446.

Kvas, A. & Mayer-Gür, T., 2019. GRACE gravity field recovery with background model uncertainties, *J Geod,* **93,** 2543–2552.

Landerer, F.W., *et al.*, 2020. Extending the global mass change data record: GRACE follow-on instrument and science data performance, *Geophys. Res. Lett.,* **47,** doi:10.1029/2020GL088306.em

Loomis, B.D., Felikson, D., Sabaka, T.J. & Medley, B., 2021. High-spatial-resolution mass rates from GRACE and GRACE-FO: global and ice sheet analyses, *J. geophys. Res.,* **126** , doi:10.1029/2021JB023024.

Noll, C.E., *et al.*, 2019. Information resources supporting scientific research for the international laser ranging service, *J. Geod.,* **93,** 2211–2225.

Poropat, L., Kvas, A., Mayer-Gürr, T. & Dobslaw, H., 2020. Mitigating temporal aliasing effects of high-frequency geophysical fluid dynamics in satellite gravimetry, *Geophys. J. Int.,* **220**(1), 257–266.

Ray, R.D., Rowlands, D.D. & Egbert, G.D., 2003. Tidal models in a new era of satellite gravimetry, *Space Sci. Rev.,* **108,** 271–282.

Rodell, M., Famiglietti, J.S., Wiese, D.N., Reager, J.T., Beaudoing, H.K., Landerer, F.W. & Lo, M.-H., 2018. Emerging trends in global freshwater availability, *Nature,* **557,** 651–659.

Sasgen, I., *et al.*, 2020. Return to rapid ice loss in Greenland and record loss in 2019 detected by the GRACE-FO satellites, *Commun. Earth Environ.,* **1,** doi:10.1038/s43247-020-0010-1.

Schindelegger, M., Harker, A.A., Ponte, R.M., Dobslaw, H. & Salstein, D.A., 2021. Convergence of daily GRACE solutions and models of submonthly ocean bottom pressure variability, *J. geophys. Res.,* **126,** doi:10.1029/2020JC017031.

Schulzweida, U., 2022. *CDO User Guide 2.1.0,* Zenodo , doi:10.5281/zenodo.7112925.

Shihora, L., Sulzbach, R., Dobslaw, H. & Thomas, M., 2021. Self-attraction and loading feedback on ocean dynamics in both shallow water equations and primitive equations, *Ocean Modell.,* **169,** doi:10.1016/j.ocemod.2021.101914.

Shihora, L., Balidakis, K., Dill, R. & Dobslaw, H., 2022a. *Atmosphere and Ocean Non-Tidal Dealiasing Level-1B (AOD1B) Product RL07. GFZ Data Services,* doi:10.5880/GFZ.1.3.2022.003.

Shihora, L., Balidakis, K., Dill, R. & Dobslaw, H., 2022b. Non-tidal background modelling for satellite gravimetry based on operational ECMWF and ERA5 reanalysis data: AOD1B RL07, *J. geophys. Res.,* **127,** doi:10.1029/2022JB024360.

Sulzbach, R., Dobslaw, H. & Thomas, M., 2021. High-resolution numerical modeling of barotropic global ocean tides for satellite gravimetry, *J. geophys. Res.,* **126** , doi:10.1029/2020JC017097.

Swenson, S. & Wahr, J., 2002. Estimated effects of the vertical structure of atmospheric mass on the time-variable geoid, *J. geophys. Res.,* **107,** ETG4–1-ETG4-11.

Tapley, B. D., Bettadpur, S., Watkins, M. & Reigber, C., 2004. The gravity recovery and climate experiment: mission overview and early results, *Geophys. Res. Lett.,* **31,** doi:10.1029/2004GL019920.

Tapley, B.D., *et al.*, 2019. Contributions of GRACE to understanding climate change, *Nat. Clim. Chang.,* **9,** 358–369.

Velicogna, I. & Wahr, J., 2006. Measurements of time-variable gravity show mass loss in Antarctica, *Science,* **311**(7668), 1754–1756.

Zenner, L., Gruber, T., Jäggi, A. & Beutler, G., 2010. Propagation of atmospheric model errors to gravity potential harmonics—impact on GRACE de-aliasing, *Geophys. J. Int.,* **182**(2), 797–807.

Zhao, M., Ponte, R.M., Penduff, T., Close, S., Llovel, W. & Molines, J., 2021. Imprints of ocean chaotic intrinsic variability on bottom pressure and implications for data and model analyses, *Geophys. Res. Lett.,* **48** , doi:10.1029/2021GL096341.